ORIGINAL RESEARCH

Analyses of protein corona on bare and silica-coated gold nanorods against four mammalian cells

Minakshi Das[1]
Dong Kee Yi[2]
Seong Soo A An[1]

[1]Department of Bionanotechnology, Gachon University, Seongnam, Republic of Korea; [2]Department of Chemistry, Myongji University, Yongin, Republic of Korea

Abstract: The purpose of this study was to investigate the mechanisms responsible for the toxic effects of gold nanorods (AuNRs). Here, a comprehensive study was performed by examining the effects of bare (uncoated) AuNRs and AuNRs functionalized with silica (SiO_2-AuNRs) against various mammalian cell lines, including cervical cancer cells, fibroblast cells, human umbilical vein endothelial cells, and neuroblastoma cells. The interactions between AuNRs and mammalian cells were investigated with cell viability and mortality assays. Dihydrorhodamine-123 assay was carried out for evaluating reactive oxygen species (ROS) generation, along with mass spectroscopy analysis for determining the composition of the protein corona. Our results suggest that even the lowest concentrations of AuNRs (0.7 µg/mL) induced ROS production leading to cell mortality. On the other hand, cellular viability and ROS production were maintained even at a higher concentration of SiO_2-coated AuNRs (12 µg/mL). The increased production of ROS by AuNRs seemed to cause the toxicity observed in all four mammalian cell types. The protein corona on the bare AuNRs did not appear to reduce ROS generation; however, different compositions of the protein corona on bare and SiO_2-coated AuNRs may affect cellular behavior differently. Therefore, it was determined that SiO_2-coated AuNRs would be more advantageous than bare AuNRs for cellular applications.

Keywords: gold nanorods, silica coating, oxidative stress, mammalian cells, cell toxicity, protein corona

Introduction

Nanoparticles are comparable in size with many organic entities and subcellular compounds; thus, nanoparticles may interact with a range of biological systems, depending on composition and specific application. Such interactions may be helpful for treating various diseases; however, the use of these nanoparticles could also have adverse effects leading to toxicity and cellular death. Numerous studies have described the interactions of gold nanorods (AuNRs) with various mammalian cells.[1–3] AuNRs have been described as not entering the nucleus but remaining entrapped in the vesicles. However, the exact pathway for AuNRs is not known. In general, larger particles move through cells via phagocytosis, whereas receptor-mediated endocytosis is considered the most important working mechanism.[4]

While it is essential to understand the potential benefits of AuNRs on cellular behavior, it is equally important to address any toxicity concerns. Thus, another key challenge is determining the exact mechanism responsible for cellular toxicity. Several biochemical tests have been applied to determine the levels of nanomaterials that were toxic to cell lines, using viability, reactive oxygen species (ROS), and

Correspondence: Seong Soo A An
Department of Bionanotechnology, Gachon Medical Research Institute, Gachon University, Sungnam-si, Gyeonggi-do, 461 701, Republic of Korea
Tel +82 31 750 8755
Fax +82 31 750 8755
Email seongaan@gachon.ac.kr

Dong Kee Yi
Department of Chemistry, Myongji University, Yongin, 449 728, Republic of Korea
Tel +82 31 330 6178
Email vitalis@mju.ac.kr

genotoxicity assays.[5] Two major components were deemed to be responsible for the toxic effects of AuNRs covered with surface ligands, which were identified as cetyltrimethylammonium bromide (CTAB) bilayers and residual or desorbed reagent-free CTAB molecules. This surfactant was shown to be poisonous to cells, even at low concentrations.[1] In addition, ROS formation and cellular oxidative stress were proposed as possible mechanisms for nanoparticle toxicity.[6–8] It was reported that oxidative stress by nanoparticles was correlated with increased ROS.[9] Furthermore, the interaction of nanomaterials with the biological fluids creating protein layers on the surface of the nanomaterials, termed the "protein corona", has garnered much attention. Therefore, in the present study, we investigated the interaction of nanomaterials and mammalian cells to determine the cytotoxicity mechanism induced by AuNRs and AuNRs functionalized with a silica coating (SiO$_2$-AuNRs) in four different cell lines: cervical cancer cells (HeLa), fibroblast cells (FY-11), human umbilical vein endothelial cells (HUVECs), and neuroblastoma cells (SH-SY5Y). Cytotoxicity was analyzed using several cell viability assays, including the 3-(4,5-dimethyl-2-thiazolyl)-2,5-diphenyltetrazolium bromide (MTT) assay and a CellTiter-Glo® assay. For this evaluation, we focused on the oxidative effects induced by nanomaterials, which resulted in decreased cellular viability and increased cellular death. In addition, mass spectroscopy (MS) analysis indicated involvement of the protein corona layer formed on the AuNRs and SiO$_2$-AuNRs in inducing free-radical production inside the cells.

Materials and methods

Materials

Gold (III)chloride trihydrate (HAuCl$_4$), sodium borohydride (NaBH$_4$), CTAB, ascorbic acid (AA), and silver nitrate (AgNO$_3$) were purchased from Sigma-Aldrich (St Louis, MO, USA). 3-Mercaptopropyltrimethoxy silane (MPS) and ammonium hydroxide (NH$_4$OH) were purchased from Aldrich (Milwaukee, WI, USA). Ultrapure deionized water was used for preparing all solutions and subsequent experiments.

Phosphate-buffered saline (PBS, pH 7.4), MTT assay reagent, and dihydrorhodamine-123 (DHR) were purchased from Sigma-Aldrich. Dulbecco's Modified Eagle's Medium (DMEM) and DMEM/F12 were purchased from Gibco-Invitrogen (Grand Island, NY, USA). Endothelial Cell Basal Medium-2 (EBM-2) was purchased from Lonza (Walkersville, MD, USA). Heat-inactivated fetal bovine serum (FBS), penicillin and streptomycin, and other tissue culture reagents were purchased from Thermo Scientific (Waltham, MA, USA). The CellTiter-Glo® assay kit was purchased from Promega (Madison, WI, USA).

Synthesis of AuNRs

AuNRs were synthesized according to previously described methods.[10] Briefly, 0.25 mL of aqueous 0.01 M HAuCl$_4$·3H$_2$O solution and 7.5 mL of 0.10 M CTAB were mixed in a conical flask, after which 0.6 mL of 0.01 M ice-cold NaBH$_4$ solution was added to the flask. Following the addition of NaBH$_4$, the clear white solution turned to a brick-brown color, indicating the formation of Au nanoparticles. This solution was aged for 2.5 hours at 25°C–28°C to form the seed solution.

Meanwhile, in another beaker, 9.5 mL of 0.1 M CTAB, 0.4 mL of 0.01 M HAuCl$_4$·3H$_2$O, and 0.03 mL of 0.01 M AgNO$_3$ were mixed. A volume of 0.064 mL of 0.1 M ascorbic acid was added to the mixture, which immediately turned the solution from orange–yellow to colorless. Finally, 0.010 mL of the seed solution was added, the solution was gently mixed for 10 seconds, and then it was left undisturbed for 24 hours.

Synthesis of SiO$_2$-AuNRs

SiO$_2$-AuNRs were synthesized according to a previously published method.[11–14] A volume of 3 mL of the AuNRs solution was centrifuged to remove excess CTAB and was redispersed in distilled water. A solution containing 5.58 µL of MPS in 20 mL of ethanol was prepared, and 80 µL of the solution was added to the AuNRs solution under vigorous magnetic stirring for 30 minutes to achieve a silica coating of intermediate thickness (around 3 nm). A volume of 20 µL of NH$_4$OH (pH 9) was then added, and the solution was vigorously stirred for 1 hour. The solution was washed three times with ethanol by centrifugation and was treated with 70% ethanol to eliminate any bacteria. A schematic representation of the AuNRs and SiO$_2$-AuNR synthesis process is shown in Figure 1.

Characterizations

Transmission electron microscopy (TEM) was performed using a JEM-3010 microscope (JEOL, Tokyo, Japan) operating at 300 kV. TEM samples were prepared by depositing 10 µL of the SiO$_2$-AuNRs suspension on carbon-coated copper grids, which was followed by the removal of excess solution and vacuum drying in an oven for 24 hours. Ultraviolet-visible (UV-Vis) spectra of the SiO$_2$-AuNRs were measured using an Optizen 2120 UV spectrophotometer
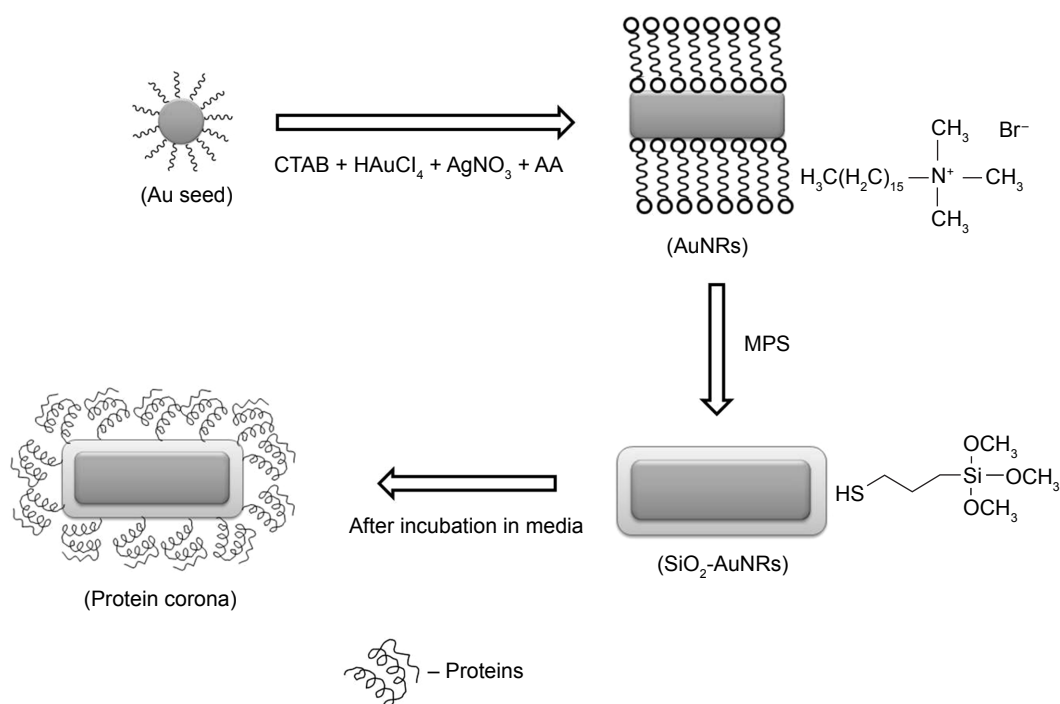
Figure 1 Schematic representation of AuNRs and SiO$_2$-AuNRs synthesis along with protein corona formation.
Abbreviations: CTAB, cetyltrimethylammonium bromide; AA, ascorbic acid; AuNRs, gold nanorods; MPS, mercaptopropyltrimethoxy silane; SiO$_2$-AuNRs, gold nanorods functionalized with silica.

(Mecasys, Daejeon, Korea) from 400 nm to 1,000 nm in 1 cm cuvettes. Zeta potential measurements were conducted using a Zetasizer Nano ZS system (Malvern Instruments, Malvern, UK).

Cell culture and treatment with AuNRs/SiO$_2$-AuNRs

FY-11 cells were cultured in DMEM containing 10% (v/v) FBS and 1% (w/v) penicillin/streptomycin at 37°C in a humidified atmosphere of 5% CO$_2$ for 24 hours. Then, cells were seeded at a density of 2×10^4 cells/well in flat-bottom 96-well plates (SPL Life Sciences, Seoul, Korea) and maintained at the same temperature and atmospheric conditions for up to 24 hours to allow cells to attach to the bottom of the plate. The cells were then washed with PBS and treated with AuNRs and SiO$_2$-AuNRs in a serum-free medium at concentrations ranging from 0.7 µg/mL to 12 µg/mL for 24 hours. After 24 hours, the medium was removed and the cells were washed twice with PBS to remove excess NRs. Cells cultured with NR-free medium served as control samples.

Cell viability analysis using MTT assay

The effect of AuNRs and SiO$_2$-AuNRs on FY-11 cell viability was evaluated using an MTT colorimetric assay, as described in previous studies.[15] MTT solution (approximately 0.5 mg/mL) was added to wells containing fresh medium and previously cultured cells. The cultures were incubated at 37°C for 2 hours. Formazan crystals were then dissolved in dimethyl sulfoxide by discarding the medium. UV absorbance was measured using a microplate reader, and the data were interpreted as the percentage of viable cells relative to the control. The same procedure was repeated for HeLa cells, but for the SH-SY5Y and HUVEC cells, DMEM/F12 and EBM-2 medium, respectively, was used for culturing the cells.

CellTiter-Glo® assay of cell viability

The CellTiter-Glo® assay was performed according to the manufacturer's protocol. The previously described culture procedures were repeated for the HeLa cells. DMEM/F12 and EBM-2 medium was used for culturing the SH-SY5Y and HUVEC cells, respectively.

Cell mortality assay

Cell mortality was assessed as previously described[6] using a Trypan blue assay (Sigma). The FY-11 cells were plated in 12-well plates, with each well containing 2×10^4 cells/well. The cells were treated with various concentrations of AuNRs and SiO$_2$-AuNRs (0.7, 1.5, 3, 6, and 12 µg/mL) that were added to the culture medium. Cells cultured in

nanoparticle-free medium were used as the control. After 24 hours, the supernatant was collected, and the cells were detached with 300 µL of trypsin–ethylenediaminetetraacetic acid solution. The mixture, consisting of the supernatant and detached cells, was centrifuged at 1,200 rpm for 5 minutes. The obtained pellet was then dispersed in 500 µL of Trypan blue. After staining for 5 minutes, the cells were counted using a Countess Automated Cell Counter (Invitrogen, Grand Island, NY, USA). Cell mortality (%) was expressed in terms of dead cell number/total cell number. This procedure was repeated for the HeLa, SH-SY5Y, and HUVEC cell lines.

Measurement of intracellular ROS

ROS generation was determined using DHR-123, as described previously.[7] Cells were plated into 96-well plates. After 24 hours of incubation, the medium was discarded, and the cells were preincubated with 100 µL of 10 µM DHR-123 solution and the growth medium at 5% CO_2, 95% air at 37°C for 30 minutes. Following the incubation period, the medium was removed and cells were washed three times with PBS. The cells were then exposed to AuNRs and SiO_2-AuNRs at concentrations of 0.75, 1.5, 3, 6, and 12 µg/mL for 24 hours. The fluorescence intensity of each well was analyzed using a microplate reader (Victor 3; Perkin-Elmer, Waltham, MA, USA) with an excitation filter of 485 nm and an emission filter of 535 nm. This procedure was repeated for the HeLa, SH-SY5Y, and HUVEC cell lines.

Identification of the protein corona using MS

AuNRs and SiO_2-AuNRs were incubated in DMEM and Roswell Park Memorial Institute (RPMI) medium for 1 hour at 37°C with rotation. After 1 hour, the samples were centrifuged at 18,000× g for 30 minutes, and the supernatant was discarded. PBS was then added to resuspend the AuNRs and SiO_2-AuNRs. This washing procedure was repeated three times, and the samples were then sent for MS determination at Diatech (Korea) to confirm the formation of the protein corona.

Statistical analysis

Statistical analysis performed was based on three replicates of each experiment. The significant differences were examined using Student's *t*-test. Significance was analyzed at $P < 0.05$.

Results

Characterization of AuNRs and SiO_2-AuNRs

The CTAB-stabilized AuNRs were encapsulated with a CTAB bilayer on their surface. For typical SiO_2-AuNRs synthesis, removal of the unbound CTAB is essential; therefore, the washing step must be performed very carefully. Here, with the use of a silane-coupling agent, uniform layers of SiO_2 were formed, with an aspect ratio of 3.0±0.2. A uniform silica coating over AuNRs can be seen in Figure 2.

Characterization UV-Vis spectra

The UV-Vis spectra of the AuNRs before and after coating with SiO_2 showed that the physiochemical properties of the AuNRs are altered (Figure 3). The prepared AuNRs have a weak transverse plasmon band at 522 nm and a strong longitudinal plasmon band at 630 nm, whereas for the SiO_2-AuNRs, the longitudinal surface plasmon band was red-shifted by 5 nm. This shift is attributed to an increase in the local refractive index of the medium surrounding the AuNRs after the formation of SiO_2 shell.

Characterization of zeta potential

The AuNR surface is positively charged due to the presence of polycations; thus, the zeta potential value was observed to be
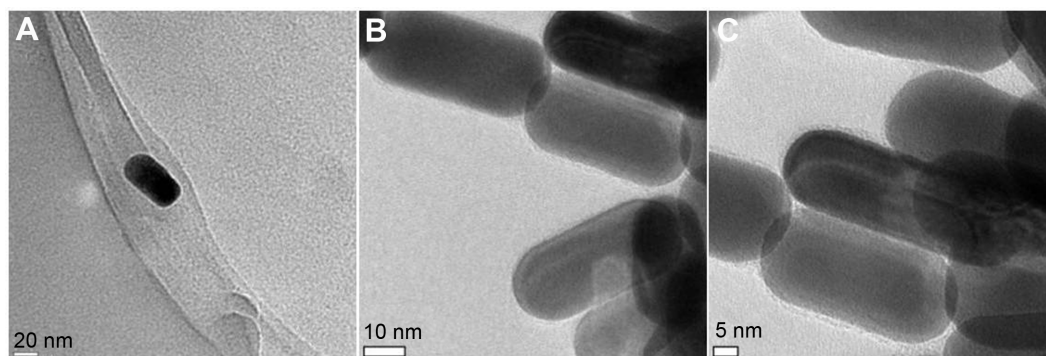

Figure 2 Transmission electron microscope images of AuNRs (**A**) and intermediate SiO_2-AuNRs, showing a silica shell thickness of around 3 nm (**B** and **C**).
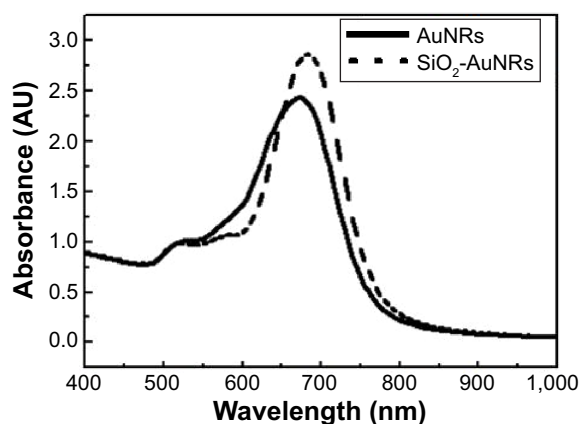
Figure 3 UV-Vis spectra of AuNRs and SiO$_2$-AuNRs.
Note: AuNRs show a weak transverse plasmon band at 522 nm and a strong longitudinal plasmon band at 630 nm, whereas for the SiO$_2$-AuNRs, the longitudinal surface plasmon band was red shifted by 5 nm.
Abbreviations: AuNRs, gold nanorods; SiO$_2$-AuNRs, gold nanorods functionalized with silica; UV-Vis, ultraviolet-visible spectroscopy.

66.2 mV, whereas after coating with SiO$_2$, the surface becomes negatively charged with a value of −25.7 mV, as shown in Figure 4A and B. These zeta potential values confirm the stability and decreased aggregation of the AuNRs and SiO$_2$-AuNRs, and therefore the zeta potential results confirm the coating of the AuNR surfaces with SiO$_2$.

Cellular viability based on the CellTiter-Glo® assay

The mitochondrial function and cellular viability of the HeLa, FY-11, SH-SY5Y, and HUVEC cells, in the presence of AuNRs and SiO$_2$-AuNRs, are shown in Figure 5A–D. AuNRs induced toxicity even at the lowest concentration, whereas SiO$_2$-AuNRs maintained more than 80% of cellular viability for all concentrations. Similar viability was observed in the case of all four cell types.
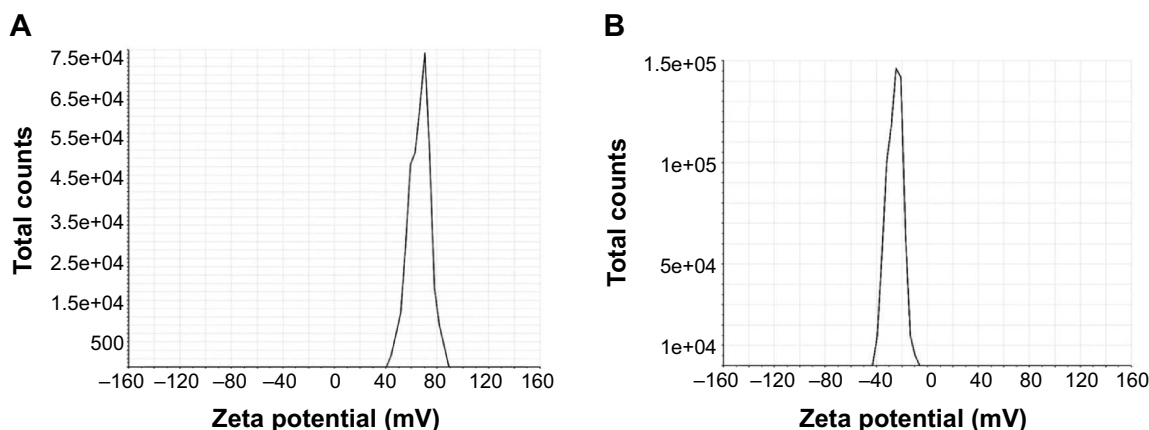
Cellular viability based on MTT assay

The cytotoxicity of AuNRs incubated with the cells was shown to be quite high, decreasing metabolic activity by about 50%, whereas even at high SiO$_2$-AuNRs concentrations, 80% viability was maintained, as shown in Figure 6A–D. As shown in Figure 6, the toxic effect of the AuNRs on mitochondrial activity increased with increasing concentrations.

Cellular mortality

In this study, cellular mortality was monitored using the Trypan blue assay, where dead cells were stained blue, while live cells remained unchanged. Mortality was expressed as the ratio of dead cells to total cells. Here, greater cell mortality (%) was observed in the presence of AuNRs, whereas cellular mortality was relatively low with the SiO$_2$-AuNRs. As shown in Figure 7, the HeLa, FY-11, SH-SY5Y, and HUVEC cells had an average mortality percentage of around 0.4%, even at the highest concentration of 12 µg/mL SiO$_2$-AuNRs, whereas mortality even at lower concentrations of AuNRs was quite high at around 0.3% for all cells. For the SiO$_2$-AuNRs, cellular mortality remained almost similar to the control for all cells, while the AuNRs exhibited relatively high cell mortality.

NR-induced ROS generation

The formation of intracellular free-radical levels could induce oxidative damage to cellular components, ultimately resulting in necrosis. The potential of AuNRs and SiO$_2$-AuNRs to induce oxidative stress was determined by measuring the ROS levels. Significant ROS elevation was observed for the HeLa, FY-11, SH-SY5Y, and HUVEC cells after 24 hours of exposure to the AuNRs and SiO$_2$-AuNRs at concentrations including 0.7, 1.5, 3, 6, and 12 µg/mL.

Figure 4 Surface charge analysis of nanorods by zeta potential measurement.
Note: (**A**) AuNRs possessed high positive surface charge with a value of 66.2 mV and (**B**) SiO$_2$-AuNRs possessed negative surface charge with a value −25.7 mV.
Abbreviations: AuNRs, gold nanorods; SiO$_2$-AuNRs, gold nanorods functionalized with silica.
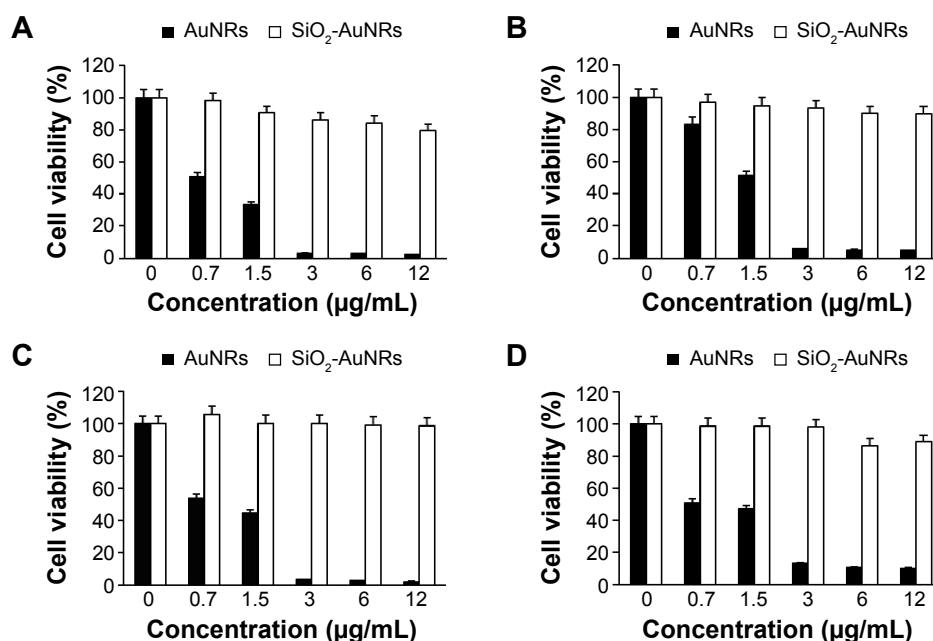
Figure 5 Shows AuNRs and SiO$_2$-AuNRs impact on cellular viability of HeLa (**A**), FY-11 (**B**), SH-SY5Y (**C**) and HUVEC (**D**) cells as determined by CellTiter-Glo® assay.
Notes: AuNRs and SiO$_2$-AuNRs were incubated with cells for 24 h at 0.7–12 µg/ml. Control group was treated with media.
Abbreviations: AuNRs, gold nanorods; SiO$_2$-AuNRs, gold nanorods functionalized with silica; FY-11, fibroblast cells; HeLa, cervical cancer cells; SH-SY5Y, neuroblastoma cells; HUVEC, human umbilical vein endothelial cell.

These results demonstrate that the formation of free radicals is significantly induced by AuNRs and SiO$_2$-AuNRs in different cell lines. Based on these obtained results, for 12 hours, a negligible increase in the production of hydrogen peroxide (H$_2$O$_2$), hydroxyl radical (•OH), and superoxide anion (O$_2$•$^-$) was observed from the AuNRs, whereas the production from

the SiO$_2$-AuNRs was almost similar to the control. After an 18-hour incubation period, the AuNRs increased ROS production by an average of 20%. Cells containing SiO$_2$-AuNRs exhibited a slight increase in ROS by around 5%, which was similar to the control. Finally, after 24 hours of incubation, it was observed that cells treated with AuNRs produced a higher
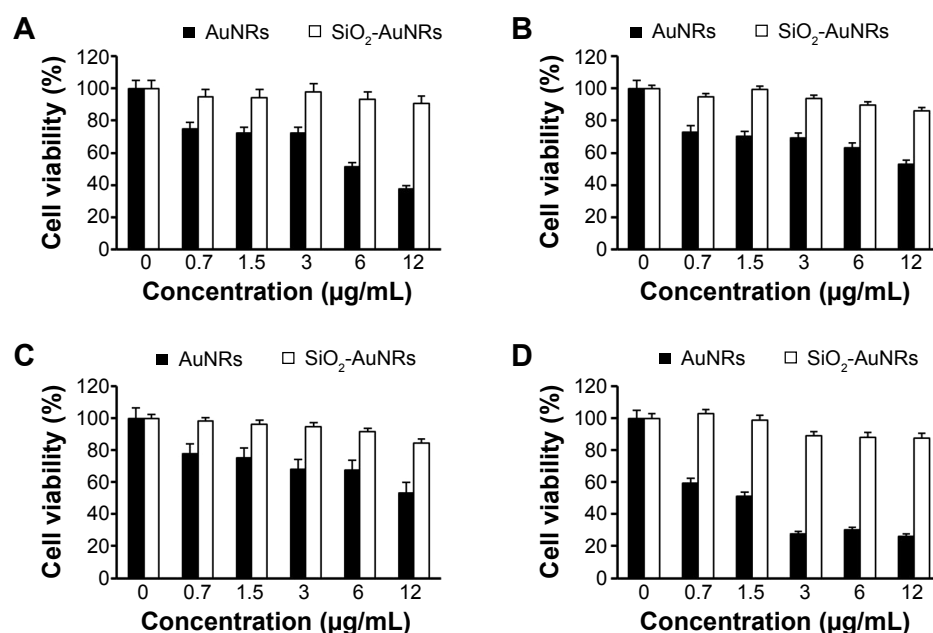
Figure 6 Cell viability of HeLa (**A**), FY-11 (**B**), SH-SY5Y (**C**) and HUVEC (**D**) cells after exposure to increasing doses of AuNRs and SiO$_2$-AuNRs for 24 h, as determined by MTT assay.
Note: The data represents AuNRs to be significantly toxic than SiO$_2$-AuNRs.
Abbreviations: AuNRs, gold nanorods; SiO$_2$-AuNRs, gold nanorods functionalized with silica; FY-11, fibroblast cells; HeLa, cervical cancer cells; SH-SY5Y, neuroblastoma cells; HUVEC, human umbilical vein endothelial cell; MTT, 3-(4,5-dimethyl-2-thiazolyl)-2,5-diphenyltetrazolium bromide.

Figure 7 Cell mortality assay of HeLa (**A**), FY-11 (**B**), SH-SY5Y (**C**) and HUVEC (**D**) cells.
Note: AuNRs and SiO$_2$-AuNRs having concentration of 0.7, 1.5, 3, 6 and 12 μg/ml were exposed to the cells for 24 h. The cell mortality was measured with trypan blue. The control group was treated with media only.
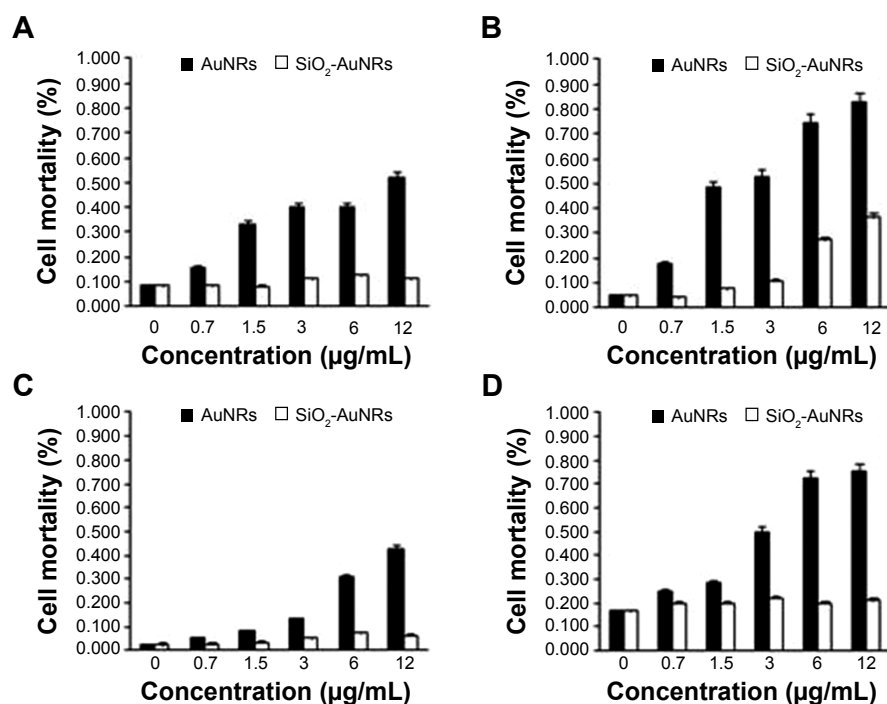**Abbreviations:** AuNRs, gold nanorods; SiO$_2$-AuNRs, gold nanorods functionalized with silica; FY-11, fibroblast cells; HeLa, cervical cancer cells; SH-SY5Y, neuroblastoma cells; HUVEC, human umbilical vein endothelial cell.

percentage of H$_2$O$_2$, •OH, and O$_2$$^{•-}$ than those treated with SiO$_2$-AuNRs did, as shown in Figure 8, which led to cellular death. AuNRs produced almost 60% of free radicals in all cell lines, whereas the production induced by the SiO$_2$-AuNRs remained around 20%, resulting in greater cellular viability.

Effects of the protein corona on NRs

To present a comprehensive characterization, MS analysis was performed to determine the biomolecular entities formed

by dispersing AuNRs and SiO$_2$-AuNRs into the cell culture medium. Table 1 reports the number of proteins attached to AuNRs and SiO$_2$-AuNRs incubated in DMEM and RPMI.

This analysis showed that in both types of cell culture medium (DMEM and RPMI), the total number of proteins attached to the AuNR surface was less than that of the SiO$_2$-AuNR surface. As previously shown,[16] this nano–bio interface is due to three dynamically interacting components: 1) the surface of NRs whose characteristics are determined
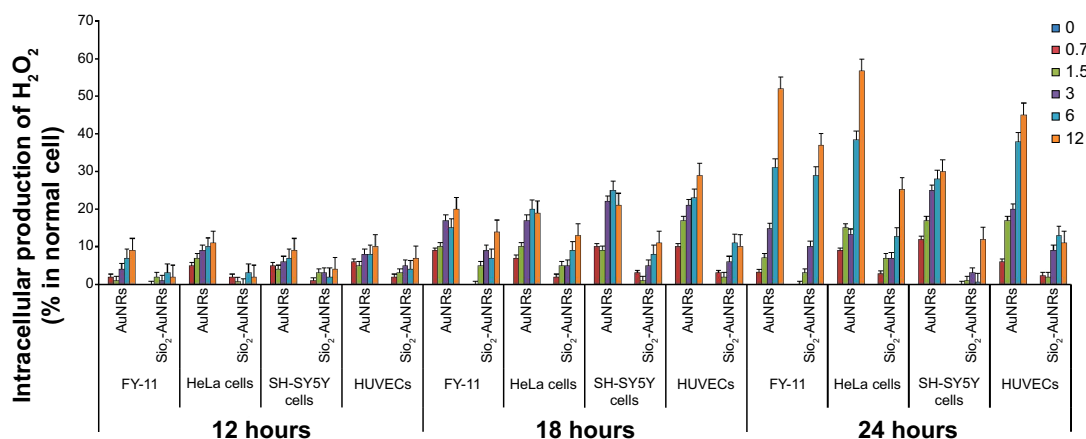
Figure 8 The expression of ROS in FY-11, HeLa, SH-SY5Y and HUVEC cells exposed for 12, 18 and 24 h to different concentrations of AuNRs and SiO$_2$-AuNRs.
Notes: AuNRs and SiO$_2$-AuNRs concentrations are measured in μg/ml. Bar graph indicates statistically significant differences between AuNRs and SiO$_2$-AuNRs. All cells with media served as controls.
Abbreviations: AuNRs, gold nanorods; SiO$_2$-AuNRs, gold nanorods functionalized with silica; FY-11, fibroblast cells; HeLa, cervical cancer cells; SH-SY5Y, neuroblastoma cells; HUVECs, human umbilical vein endothelial cells; ROS, reactive oxygen species.

Table 1 Total number of proteins attached to the surface of AuNRs and SiO$_2$-AuNRs

Medium	Sample	Total proteins	Within criteria	Without criteria
DMEM	AuNRs	146	102	44
		100	66	34
RPMI	SiO$_2$-AuNRs	153	106	47
		122	84	42

Abbreviations: DMEM, Dulbecco's Modified Eagle's Medium; RPMI, Roswell Park Memorial Institute; AuNRs, gold nanorods; SiO$_2$-AuNRs, gold nanorods functionalized with silica.

by their physiochemical composition, 2) the changes that occur following the solid–liquid interface when the particle interacts with components in the surrounding medium, and 3) the contact area of the solid–liquid interface with its biological substrates. Specific NR properties have been shown to greatly contribute to the NR interactions with medium.[17] For example, certain NR properties may result in increased adsorption of ions, proteins, organic materials,

and detergents, which permits double-layer formation and minimizes the free surface energy by surface modification. There are several factors affecting the protein corona formation, including protein–AuNRs interactions, protein–protein interactions, and protein–medium interactions.[18]

As shown in Figure 9, the DMEM and RPMI mediums encouraged the attachment of a comparable number of proteins. The major difference observed was with the surface
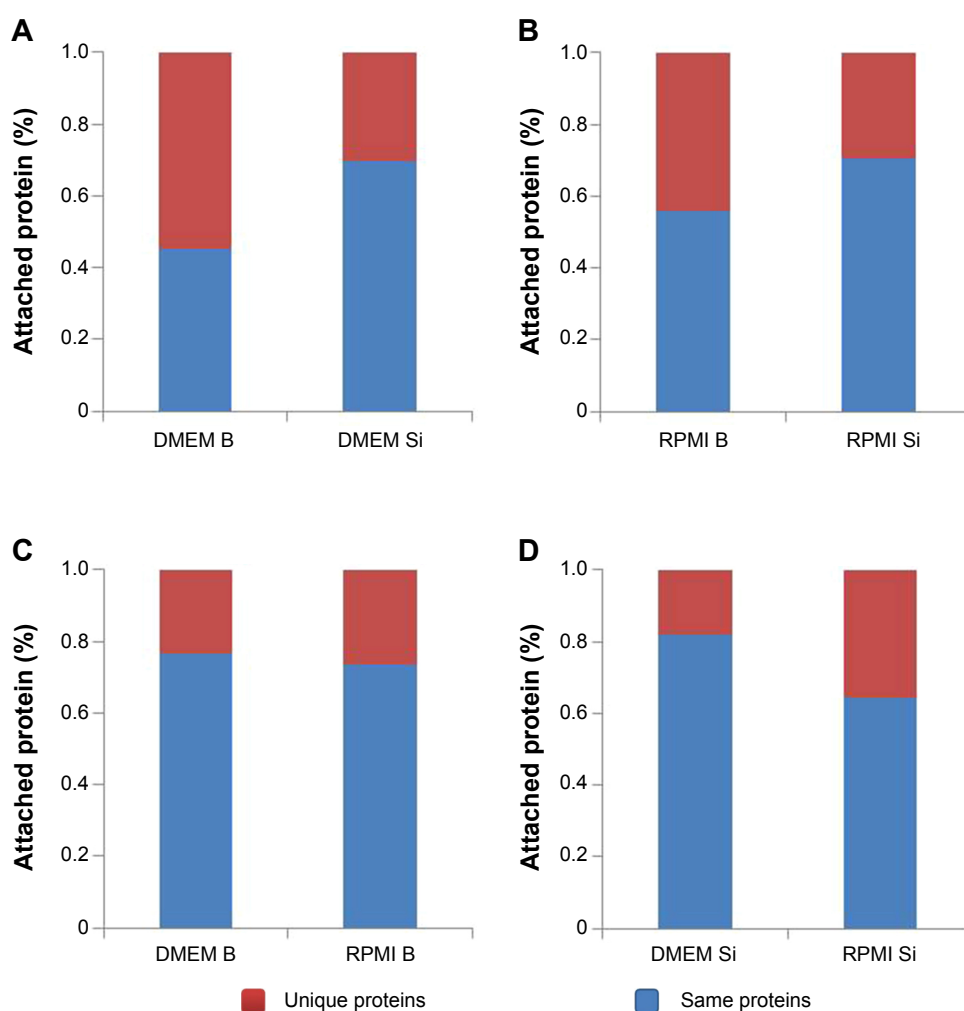
Figure 9 Proteins attachment on AuNRs and SiO$_2$-AuNRs surfaces incubated in DMEM and RPMI medium for 1 h.
Notes: (**A**) Represents the attachment of larger numbers of unique proteins (50%) on DMEM incubated AuNRs, whereas on DMEM incubated SiO$_2$-AuNRs a lesser number of unique proteins are attached. (**B**) Represents the attachment of a larger number of unique proteins (50%) on RPMI medium incubated AuNRs, whereas on RPMI medium incubated SiO$_2$-AuNRs a lesser number of unique proteins are attached. (**C**) and (**D**) Represents the number of unique proteins attached on DMEM and RPMI medium incubated AuNRs and SiO$_2$-AuNRs, which are almost similar. Hence, it is apparent that the attachment solely depends on the surface properties and charges, rather than differences in the medium.
Abbreviations: DMEM, Dulbecco's Modified Eagle's Medium; RPMI, Roswell Park Memorial Institute; B, bare; Si, silica.

charges, as the number of unique proteins attached in the AuNRs increases by approximately 50% more than that of the SiO$_2$-AuNRs. The difference in surface charge encouraged the formation of different hybrid bionanostructures that, in turn, exerted different biological effects when interacting with cells. Furthermore, as shown in Figure 10, the unique proteins that got attached to the AuNRs were cell matrix adhesion proteins. These cell matrix adhesion proteins were present in DMEM- and RPMI-incubated AuNRs, whereas they were absent in DMEM- and RPMI-incubated SiO$_2$-AuNRs.

The main species of cell matrix adhesion proteins that were adsorbed onto the metallic NR surfaces were identified as important proteins involved in key biological processes (Table 2), which included alpha actinin 1 (actin-binding proteins, several roles in several cells), fibronectin (extracellular matrix glycoprotein, binds to integrins and plays a role in cell adhesion, growth, migration, differentiation, wound healing, and embryonic growth), angiotensin (peptide hormone, causes vasoconstriction and increase in blood pressure), nidogen (basement membrane glycoprotein, plays a role in cell–extracellular matrix interactions), and vitronectin (glycoprotein found in serum and extracellular matrix, plays a role in cell adhesion and spreading).

Discussion

Interest in the use of AuNRs for biomedical applications has grown due to their unique physiochemical properties; however, their current use has been limited because of major concerns over their toxicity. AuNRs are toxic to cells due to the presence of CTAB, which is required for AuNR stabilization. Therefore, surface functionalization, such as with SiO$_2$, has been used in an effort to reduce AuNR toxicity.

For AuNRs, the intensity of the longitudinal plasmon band corresponding to the long axis of the NRs has been shown to be much higher than that of the transverse plasmon band corresponding to the short axis of the NRs, because of the enhanced surface electric field due to surface plasmon excitation.[15]
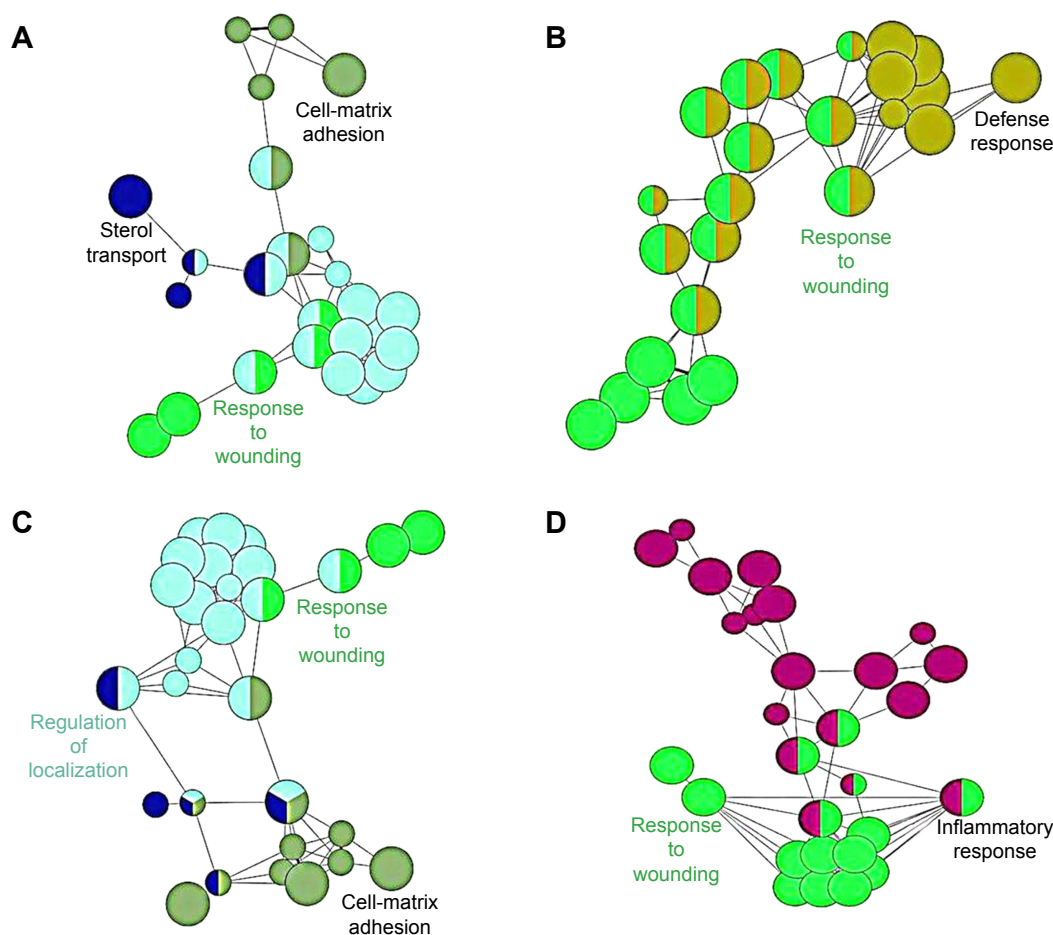
Figure 10 Unique proteins attached on the surface of DMEM (**A**, **B**) and RPMI medium (**C**, **D**) incubated AuNRs and SiO$_2$-AuNRs.
Notes: (**A**) Represents the presence of cell matrix adhesion proteins on AuNRs; (**B**) represents the absence of cell matrix adhesion proteins on SiO$_2$-AuNRs; (**C**) represents the presence of cell matrix adhesion proteins on AuNRs; (**D**) represents the absence of cell matrix adhesion proteins on SiO$_2$-AuNRs.
Abbreviations: DMEM, Dulbecco's Modified Eagle's Medium; RPMI, Roswell Park Memorial Institute; AuNRs, gold nanorods; SiO$_2$-AuNRs, gold nanorods functionalized with silica.

Table 2 List of cell matrix adhesion proteins attached to AuNRs and SiO$_2$-AuNRs surfaces

Protein	DMEM AuNRs	DMEM SiO$_2$-AuNRs	RPMI AuNRs	RPMI SiO$_2$-AuNRs
Alpha-actinin-1	10.21	Absent	10.18	Absent
Fibronectin	460.32	20.16	530.35	240.32
Angiotensin	140.33	60.26	190.32	80.29
Nidogen	10.15	Absent	20.22	Absent
Vitronectin	90.33	70.29	110.33	80.33

Abbreviations: DMEM, Dulbecco's Modified Eagle's Medium; RPMI, Roswell Park Memorial Institute; AuNRs, gold nanorods; SiO$_2$-AuNRs, gold nanorods functionalized with silica.

Therefore, in the case of SiO$_2$-AuNRs, the shift in the longitudinal plasmon band is larger than that of the transverse band, which is at a wavelength close to the characteristic band of Au nanoparticles of similar diameter.

Every particle in a mixture carries some charge, which is typically negative rather than positive. This is attributed to the presence of chemical groups on the surface of the particle, which are ionized to form a charged surface. Sometimes, ions with an opposite charge may be adsorbed to the surface, and at other times chemical compounds may be intentionally added to yield a specific charge. In this study, CTAB acts as a chemical compound that generates the charge for the AuNRs. Since the CTAB-stabilized AuNRs possess a highly positive surface charge, the wrapping of negative ions around the metal is strongly favored. Hence, a SiO$_2$ coating over the AuNRs was formed, and zeta potential analysis was performed to confirm the coating of SiO$_2$-AuNRs.

In the present study, a visible difference in cell viability was observed based on the results of the viability assays used, as different mechanisms were involved. For the MTT assay, water-soluble MTT was converted to an insoluble formazan crystal. The formazan was then solubilized by inorganic solvent, and the concentration was determined by determining the optical density at 570 nm. Alternatively, for the CellTiter-Glo® assay, a homogeneous method based on the amount of adenosine triphosphate (ATP) present, which indicates the presence of metabolically active cells, was used to determine the number of viable cells.

Typically, polycationic materials exhibit higher cytotoxicity. AuNRs stabilized with CTAB and washed once with water by centrifugation showed strong cytotoxicity due to free CTAB remaining in the solution. However, in the case of the SiO$_2$-AuNRs, more than 70% cell viability was observed even at the highest concentrations, indicating that the removal of excess CTAB and modification with SiO$_2$ contributed to a significant decrease in cytotoxicity. The SiO$_2$-AuNRs exhibited lower toxicity, which is essential for biomedical applications using AuNRs. In addition, the absence of CTAB on the AuNR surfaces has been shown to affect biological processes inside the cells, while binding to the cell membrane.[19]

Since material properties affect the kinetics of cell death, the mechanisms of nanomaterial-mediated cell toxicity may vary depending on the composition of the material each cell type interacts with. ROS generation has been suggested as an initial cellular response to nanomaterial internalization and subsequent cell death. In this study, the nanomaterial-mediated cell responses prior to cell death, specifically the production of intracellular ROS, were measured at 6 hours via the DHR assay. Our results showed that AuNRs increased the production of ROS in all cells by 60%, depending on the time, whereas ROS production for the SiO$_2$-AuNRs was negligible. These results indicated that SiO$_2$ scavenged the production of the ROS. The mechanism for the production of free radicals and its relation to toxicity are described as follows.

Typically, ROS generated by cells within an enclosed environment may easily turn into a source of cell and tissue injury. O$_2$ is essential for human survival, and aerobic energy metabolism depends upon oxidative phosphorylation, which plays a vital role through which the oxidoreduction energy of mitochondrial electron transport is eventually converted to the high-energy phosphate bond of ATP. Aerobic organisms use O$_2$ as the final electron acceptor for mitochondrial cytochrome c oxidase, which is able to catalyze the four electron reduction of O$_2$, leading to H$_2$O formation (Equation 1). During mitochondrial oxidative phosphorylation, and other electron transfer reactions, including those of the superoxide anion (O$_2{}^{\bullet-}$), hydrogen peroxide (H$_2$O$_2$) and hydroxyl radicals ($\bullet$OH) can be formed within cells (Equation 2). These reactive O$_2$ metabolites are usually collectively referred to as ROS, and their generation in a biological environment exposes most living organisms to the so-called "oxygen paradox". O$_2$ is essential for life, but it is also potentially hazardous, since ROS may become a source of cell and tissue injury.

Equation 1

In a human body, four electron reduction reactions occur, leading from O$_2$ to H$_2$O production:

1. $O_2 + e^- \rightarrow O_2^{\bullet-} (+H^+ \leftrightarrow HO_2^{\bullet})$
2. $O_2^{\bullet-} + e^- \rightarrow (O_2^{2-} + 2H^+) \rightarrow H_2O_2$
3. $H_2O_2 + e^- \rightarrow {}^{\bullet}OH + OH^-$
4. $OH + e^- \rightarrow +H^+ \rightarrow H_2O.$

Equation 2

When the human body is exposed to a foreign material (metal nanoparticles), then carbon-centered free radicals are generated by interaction with ROS:

1. $R–H + {}^{\bullet}OH \rightarrow R^{\bullet} + H_2O$ (organic radical)
2. $R^{\bullet} + O_2 \rightarrow ROO^{\bullet}$ (peroxyl radical)
3. $ROO^{\bullet} + R–H \rightarrow ROOH + R^{\bullet}$ (organic peroxide)
4. $ROOH + nanoparticle \rightarrow RO^{\bullet} + {}^{-}OH + nanoparticle$ (alkoxy radical).

Thus, the free radicals produced may be very dangerous, leading to cell death. In this study, the results obtained were different for each cell type; however, the production of intracellular ROS increased due to the presence of AuNRs, while SiO_2-AuNRs showed scavenging properties.

Based on the principles involved in ROS production, the question arises of what induces increased free-radical production within cells. Recently, many researchers have addressed the relationship between nanomaterials and biological fluid interaction. A layer formed over the nanomaterial has been defined as the "corona".[20] When NRs enter a biological fluid (medium), they are coated with proteins that may undergo conformational changes, leading to the exposure of new epitopes, altered function, and/or avidity effects.[18] The concept of the NR–protein corona is important for tuning the surface properties, charges, resistance to aggregation, and toxicity of NRs. Notably, in this study, we showed that the interactive NR surface may be prebound to chemical substances that reflect its prior history and could subsequently influence its protein adsorption kinetics.

Conclusion

The results of this study demonstrate that the AuNRs due to the presence of CTAB molecules are the source of toxicity. Providing a coating over the CTAB-coated AuNRs with alkoxysilane is one way to prevent toxicity, which explains why the overcoated rods examined in this work were far more biocompatible.

In addition, we analyzed the protein corona formed over AuNRs and SiO_2-AuNRs to determine any significant differences and to identify the cause of toxicity observed on the two types of NRs. Based on our hypothesis, we confirmed with MS that two different groups of protein corona were formed on the AuNRs and SiO_2-AuNRs, respectively. The corona formation completely depended on the material surface properties. The MS data suggested the presence of cell matrix adhesion proteins on the AuNRs, and the absence of those proteins on the SiO_2-AuNRs. Cell matrix adhesion proteins such as immunoglobulin are associated with the recognition and phagocytosis of NRs into the cells. The adsorbed proteins regulate the NR–cellular interactions, thus making them toxic or nontoxic to cells. In addition, different reports have shown that the corona could force the toxicity of materials.[20] The presence of such proteins could be the reason for excessive free-radical production in cells leading to cell death. The list of proteins involved in corona formation are mentioned in the supplementary information. Hence, we concluded that the biological impact of the AuNRs was not exactly associated with their properties but associated with the attributes of the corona NR complexes. Further studies of the protein corona and its behavior could provide a clearer picture of this relationship.

Acknowledgments

Disclosure

The authors report no conflicts of interest in this work.

References

1. Alkilany AM, Nagaria PK, Hexel CR, Shaw TJ, Murphy CJ, Wyatt MD. Cellular uptake and cytotoxicity of gold nanorods: molecular origin of cytotoxicity and surface effects. *Small*. 2009;5(6):701–708.
2. Hauck TS, Ghazani AA, Chan WC. Assessing the effect of surface chemistry on gold nanorod uptake, toxicity, and gene expression in mammalian cells. *Small*. 2008;4(1):153–159.
3. Takahashi H, Niidome T, Kawano T, Yamada S, Niidome Y. Surface modification of gold nanorods using layer-by-layer technique for cellular uptake. *J Nanopart Res*. 2008;10:221–228.
4. Kleps Conner SD, Schmid SL. Regulated portals of entry into the cell. *Nature*. 2003;422(6927):37–44.
5. Marquis BJ, Love SA, Braun KL, Haynes CL. Analytical methods to assess nanoparticle toxicity. *Analyst*. 2009;134(3):425–439.
6. Chang Y, Yang ST, Liu JH, Dong E, Wang Y, Cao A, Liu Y, Wang H. In vitro toxicity evaluation of graphene oxide on A549 cells. *Toxicol Lett*. 2011;200(3):201–210.
7. Lee JY, Park W, Yi DK. Immunostimulatory effects of gold nanorod and silica-coated gold nanorod on RAW 264.7 mouse macrophages. *Toxicol Lett*. 2012;209(1):51–57.
8. Tedesco S, Doyle H, Blasco J, Redmond G, Sheehan D. Oxidative stress and toxicity of gold nanoparticles in *Mytilus edulis*. *Aquat Toxicol*. 2010; 100(2):178–186.
9. Wang F, Gao F, Lan M, Yuan H, Huang Y, Liu J. Oxidative stress contributes to silica nanoparticle-induced cytotoxicity in human embryonic kidney cells. *Toxicol In Vitro*. 2009;23(5):808–815.
10. Sau TK, Murphy CJ. Seeded high yield synthesis of short Au nanorods in aqueous solution. *Langmuir*. 2004;20(15):6414–6420.

11. Pérez-Juste J, Correa-Duarte MA, Liz-Marzán LM. Silica gels with tailored, gold nanorod-driven optical functionalities. *Applied Surface Science*. 2004;226:137–143.

12. Cong H, Toftegaard R, Arnbjerg J, Ogilby PR. Silica-coated gold nanorods with a gold overcoat: controlling optical properties by controlling the dimensions of a gold-silica-gold layered nanoparticle. *Langmuir*. 2010;26(6):4188–4195.

13. Gorelikov I, Matsuura N. Single-step coating of mesoporous silica on cetyltrimethyl ammonium bromide-capped nanoparticles. *Nano Lett*. 2008;8(1):369–373.

14. Obare SO, Jana NR, Murphy CJ. Preparation of polystyrene- and silica-coated gold nanorods and their use as templates for the synthesis of hollow nanotubes. *Nano Lett*. 2001;1:601–603.

15. Jain PK, Lee KS, El-Sayed IH, El-Sayed MA. Calculated absorption and scattering properties of gold nanoparticles of different size, shape, and composition: applications in biological imaging and biomedicine. *J Phys Chem B*. 2006;110(14):7238–7248.

16. Tansey W, Ke S, Cao XY, Pasuelo MJ, Wallace S, Li C. Synthesis and characterization of branched poly(L-glutamic acid) as a biodegradable drug carrier. *J Control Release*. 2004;94(1):39–51.

17. Guo D, Wu C, Li X, Jiang H, Wang X, Chen B. In vitro cellular uptake and cytotoxic effect of functionalized nickel nanoparticles on leukemia cancer cells. *J Nanosci Nanotechnol*. 2008;8(5):2301–2307.

18. Nel AE, Mädler L, Velegol D, et al. Understanding biophysicochemical interactions at the nano-bio interface. *Nat Mater*. 2009;8(7):543–557.

19. Harris JM, Chess RB. Effect of pegylation on pharmaceuticals. *Nat Rev Drug Discov*. 2003;2(3):214–221.

20. Lesniak A, Fenaroli F, Monopoli MP, Åberg C, Dawson KA, Salvati A. Effects of the presence or absence of a protein corona on silica nanoparticle uptake and impact on cells. *ACS Nano*. 2012;6(7):5845–5857.

Supplementary materials

As shown in this section, a list of proteins involved in the protein corona layer due to the incubation of gold nanorods (AuNRs) (bare) and gold nanorods functionalized with silica (SiO$_2$-AuNRs) (Si) in Dulbecco's Modified Eagle's Medium (DMEM) or Roswell Park Memorial Institute (RPMI) medium is provided. As shown in the tables, "common proteins" indicates proteins involved in both DMEM-bare and DMEM-Si (Tables S3, S4, S7 and S8). On the other hand, "uncommon proteins" indicates unique proteins involved in either DMEM-bare or DMEM-Si. Similar designations

are specified for the RPMI samples (Tables S5, S6, S9 and S10).

Here, we compared DMEM-bare with DMEM-Si (Table S1) (to show the difference between "bare" and "Si" in DMEM), RPMI-bare with RPMI-Si (Table S2) (to show the difference between "bare" and "Si" in RPMI), DMEM-bare with RPMI-bare (Table S9) (to show the difference between "DMEM" and "RPMI" in bare), and DMEM-Si with RPMI-Si (to show the difference between "DMEM" and "RPMI" in Si) (Table S10).

Table S1 Protein corona list of DMEM-bare and DMEM-Si

DMEM-bare	DMEM-Si
Alpha-1-antiproteinase precursor	PREDICTED: apolipoprotein B
Protein AMBP precursor	Complement C3 preproprotein
Talin-1	Serum albumin precursor
Thyroglobulin precursor	Alpha-2-macroglobulin
Apolipoprotein E precursor	Antithrombin-III precursor
Alpha-2-antiplasmin precursor	Apolipoprotein E precursor
Apolipoprotein A-I preproprotein	Inter-alpha-trypsin inhibitor heavy chain H2
Hemoglobin fetal subunit beta	Apolipoprotein A-I preproprotein
Coagulation factor V precursor	Fibulin-1
Hyaluronan-binding protein 2	Alpha-1-antiproteinase precursor
C4b-binding protein alpha chain precursor	Alpha-2-HS-glycoprotein precursor
Kininogen-2 isoform II	Complement C4
Complement component C9 precursor	Periostin
PREDICTED: apolipoprotein B	Inter-alpha-trypsin inhibitor heavy chain H3 precursor
Tubulin, beta 1	Hemoglobin subunit alpha
PREDICTED: similar to complement component 4A	Vitronectin
PREDICTED: heparan sulfate proteoglycan 2	Heparin cofactor 2
Hemoglobin subunit beta	Prothrombin
Fibrinogen alpha chain precursor	Inter-alpha-trypsin inhibitor heavy chain H4 precursor
Hemoglobin subunit alpha	Hemoglobin fetal subunit beta
Hypothetical protein LOC510860	Angiotensinogen
Heat shock protein HSP 90-alpha	PREDICTED: complement component 4 binding protein, alpha chain-like
Serpin A3-1 precursor	Gelsolin isoform a
Factor XIIa inhibitor precursor	Protein AMBP precursor
Actin, aortic smooth muscle	Fetuin-B precursor
Tubulin alpha-4A chain	Lipopolysaccharide-binding protein precursor
Kininogen-2 isoform I	Plasma serine protease inhibitor precursor
Inter-alpha-trypsin inhibitor heavy chain H4 precursor	Complement component C9 precursor
Mannan-binding lectin serine protease 1	Actin, aortic smooth muscle
Apolipoprotein M	Coagulation factor XIII A chain precursor
Fibrinogen beta chain	Talin-1
Tenascin-X	PREDICTED: apolipoprotein B
PREDICTED: complement component 4 binding protein, alpha chain-like	Serotransferrin precursor
Collagen alpha-1 (XII) chain	Hemoglobin subunit beta
Heat shock protein HSP 90-beta	Alpha-2-antiplasmin precursor
Tubulin beta-5 chain	Phosphoglycerate kinase 1
Fibromodulin	Inter-alpha-trypsin inhibitor heavy chain H1 precursor
Fetuin-B precursor	Actin, cytoplasmic 1
Lumican precursor	L-lactate dehydrogenase B chain
Alpha-actinin-1	Apolipoprotein A-II precursor

(*Continued*)

Table S1 (*Continued*)

DMEM-bare	DMEM-Si
Vitamin D-binding protein precursor	Fibronectin
Neuropilin-1	Hypothetical protein LOC510860
Echinoderm microtubule-associated protein-like 5	Heat shock protein HSP 90-beta
PREDICTED: alpha-2-macroglobulin-like, partial	Fermitin family homolog 3
Aggrecan core protein	Phospholipid transfer protein
PREDICTED: GLIS family zinc finger 3, partial	Pyruvate kinase isozymes M1/M2
Plasma serine protease inhibitor precursor	Adenosylhomocysteinase
PREDICTED: calcium channel, voltage-dependent, L type, alpha 1S subunit-like	Complement component 8, beta polypeptide
Myosin, heavy chain 9, nonmuscle	Kininogen-2 isoform II
Glyceraldehyde-3-phosphate dehydrogenase	Kelch-like ECH-associated protein 1
Caspase-14	Alpha-enolase
tRNA-dihydrouridine synthase 1-like	PREDICTED: similar to complement component 4A
Myosin-11	Apolipoprotein M
PREDICTED: KRAB-A domain containing 2	Glyceraldehyde-3-phosphate dehydrogenase
Thrombospondin-3	Transmembrane and coiled-coil domain-containing protein 2
Neuropilin-2	Glyceraldehyde-3-phosphate dehydrogenase, testis-specific
Beta-casein precursor	Probable arginyl-tRNA synthetase, mitochondrial precursor
PREDICTED: collagen, type VI, alpha 3-like isoform 4	Serpin A3-1 precursor
Sucrase-isomaltase, intestinal	Vitamin D-binding protein precursor
Transmembrane and coiled-coil domain-containing protein 2	L-lactate dehydrogenase C isoform 1
Complement factor B precursor	Nucleolar GTP-binding protein 2
Interleukin-1 beta precursor	Thyroxine-binding globulin precursor
PREDICTED: NIMA (never in mitosis gene a)-related kinase 11	Heat shock protein HSP 90-alpha
Coagulation factor X	C4b-binding protein alpha chain precursor
SPARC-like protein 1	Neutrophil cytosol factor 1
PREDICTED: FYVE and coiled-coil domain-containing protein 1-like	Apolipoprotein D precursor
PREDICTED: thiolester containing protein II-like	Thrombospondin-1 precursor
Carbohydrate sulfotransferase 3	Zinc finger protein 668
PREDICTED: zinc finger protein 347-like	PREDICTED: mcg144546-like
C-type lectin domain family 11 member A	Dynein heavy chain 2, axonemal
Terminal uridylyltransferase 4	Coagulation factor V precursor
Nucleolar GTP-binding protein 2	Leucine-rich repeat-containing protein 49
Alpha-S1-casein precursor	Tyrosine-protein kinase BAZ1B
Collectin-11 precursor	Alpha-S1-casein precursor
Mannan-binding lectin serine protease 2	Coiled-coil domain-containing protein 71
N-acetylated-alpha-linked acidic dipeptidase 2	Pigment epithelium-derived factor precursor
Pentraxin-related protein PTX3 precursor	Clusterin preproprotein
6-Phosphogluconate dehydrogenase, decarboxylating	PREDICTED: PDS5, regulator of cohesion maintenance, homolog B (*Saccharomyces cerevisiae*)
Nidogen-1	Splicing factor 3B subunit 2
Mitochondrial-processing peptidase subunit alpha precursor	Collagen alpha-1 (XII) chain
Coiled-coil alpha-helical rod protein 1	PREDICTED: SYF2 homolog, RNA splicing factor-like, partial
Ankyrin repeat domain-containing protein 32	Carboxypeptidase B2 precursor
Complement C5a anaphylatoxin	PREDICTED: titin
von Willebrand factor	Seryl-tRNA synthetase, mitochondrial precursor
PREDICTED: hemolytic complement-like	Probable phospholipid-transporting ATPase IA
PREDICTED: ZAR1-like protein-like	Coagulation factor XIII B chain
Homeobox protein Hox-A4	26S proteasome non-ATPase regulatory subunit 1
PREDICTED: recombination activating gene 1	Filamin-C
PREDICTED: FLJ00002 protein-like	Glycine N-acyltransferase
Heat-stable enterotoxin receptor	PREDICTED: hypothetical protein
Reelin	PREDICTED: phospholipase D family, member 3-like
Hypothetical protein LOC100124506	von Willebrand factor C domain-containing protein 2-like
Kelch repeat and BTB domain-containing protein 12	Probable ATP-dependent RNA helicase DDX49
Tenascin C	PREDICTED: preferentially expressed antigen in melanoma-like
Nucleoporin p58/p45	Protein Shroom1

(*Continued*)

Table S1 (*Continued*)

DMEM-bare	DMEM-Si
PREDICTED: transcriptional regulating factor 1-like	Heat shock 70 kDa protein 1A
Endoplasmin precursor	Hypothetical protein LOC614478
PREDICTED: chloride channel protein CIC-Ka-like	Insulin-like growth factor-binding protein complex acid labile subunit
AP-1 complex subunit mu-2	PREDICTED: collagen, type VI, alpha 3-like isoform 4
TAF6-like RNA polymerase II p300/CBP associated factor	Actin-related protein 2
65 kDa subunit 6L	
Cyclin-G-associated kinase	
ARF GTPase-activating protein GIT2	
Hexokinase-1	
PREDICTED: histone cluster 1, H2bd-like	
Desmoplakin	
Ras-related protein Rap-1b precursor	
PREDICTED: transforming growth factor, beta receptor III	
Acetyl-CoA carboxylase 1	
PREDICTED: microtubule-associated protein 7-like	
PREDICTED: centrosomal protein 110 kda	
Serpin A3-7	
Voltage-dependent N-type calcium channel subunit alpha-1B	
Ribonucleoside-diphosphate reductase M1 chain	
Probable phospholipid-transporting ATPase IB	
PREDICTED: hypothetical protein	
Tubulin alpha-1D chain	
Kinesin family member C2	
Selenoprotein S	
PREDICTED: mcg144546-like	
Nucleoporin NUP188 homolog	
Actin, cytoplasmic 1	
PREDICTED: centromere protein E, 312kda	
PREDICTED: zinc finger, DHHC-type containing 18-like	
Butyrophilin-like protein 1	
PREDICTED: sodium channel protein type 11 subunit alpha-like	

Abbreviations: DMEM, Dulbecco's Modified Eagle's Medium; Si, silica; tRNA, transfer ribonucleic acid; ATP, adenosine triphosphate.

Table S2 Protein corona list of RPMI-bare and RPMI-Si

RPMI-bare	RPMI-Si
PREDICTED: apolipoprotein B	PREDICTED: apolipoprotein B
Fibronectin	Complement c3 preproprotein
Complement C3 preproprotein	Alpha-2-macroglobulin
Inter-alpha-trypsin inhibitor heavy chain H2	Serum albumin precursor
Alpha-2-macroglobulin	Inter-alpha-trypsin inhibitor heavy chain h2
Serum albumin precursor	Fibronectin
Inter-alpha-trypsin inhibitor heavy chain H3 precursor	Inter-alpha-trypsin inhibitor heavy chain H3 precursor
Thrombospondin-1 precursor	Antithrombin-III precursor
Inter-alpha-trypsin inhibitor heavy chain H1 precursor	Apolipoprotein E precursor
Gelsolin isoform a	Fibulin-1
Talin-1	Inter-alpha-trypsin inhibitor heavy chain H1 precursor
Complement C4	Complement C4
Fibulin-1	Periostin
PREDICTED: pregnancy-zone protein-like	Talin-1
Angiotensinogen	Predicted: pregnancy-zone protein-like
Thrombospondin-4 precursor	Alpha-2-HS-glycoprotein precursor
Antithrombin-III precursor	Apolipoprotein A-I preproprotein
Heparin cofactor 2	Heparin cofactor 2
Prothrombin	Gelsolin isoform a
Vitronectin	Vitronectin
Inter-alpha-trypsin inhibitor heavy chain H4 precursor	Angiotensinogen
Periostin	Complement factor B precursor
Alpha-2-HS-glycoprotein precursor	Serotransferrin precursor
Alpha-1-antiproteinase precursor	Inter-alpha-trypsin inhibitor heavy chain H4 precursor
Protein AMBP precursor	Alpha-1-antiproteinase precursor
Hyaluronan-binding protein 2	Hemoglobin fetal subunit beta
Alpha-2-antiplasmin precursor	Prothrombin
Coagulation factor V precursor	Hemoglobin subunit alpha
Tubulin, beta 1	Protein AMBP precursor
Kininogen-2 isoform II	Fetuin-B precursor
Tubulin beta-5 chain	Tubulin, beta 1
PREDICTED: apolipoprotein B	Complement C5a anaphylatoxin
PREDICTED: collagen, type VI, alpha 3-like isoform 4	Plasma serine protease inhibitor precursor
Hemoglobin fetal subunit beta	Lipopolysaccharide-binding protein precursor
Kininogen-2 isoform I	Kininogen-2 isoform II
Apolipoprotein E precursor	Fermitin family homolog 3
Tubulin alpha-4A chain	Complement component C9 precursor
Pigment epithelium-derived factor precursor	Actin, aortic smooth muscle
Cartilage oligomeric matrix protein	Thrombospondin-1 precursor
Hypothetical protein LOC510860	Alpha-2-antiplasmin precursor
Heat shock protein HSP 90-beta	Hemoglobin subunit beta
C4b-binding protein alpha chain precursor	Phospholipid transfer protein
Mannan-binding lectin serine protease 1	Complement component 8, beta polypeptide
Hemoglobin subunit beta	Fibrinogen beta chain
Fibrinogen alpha chain precursor	Alpha-fetoprotein precursor
Coagulation factor X	Thrombospondin-4 precursor
PREDICTED: complement component 4 binding protein, alpha chain-like	PREDICTED: apolipoprotein B
Fibrinogen beta chain	Properdin
Complement component C9 precursor	Hypothetical protein LOC510860
C-type lectin domain family 11 member A	C4b-binding protein alpha chain precursor
Filamin-A	Coagulation factor V precursor
Fetuin-B precursor	PREDICTED: collagen, type VI, alpha 3-like isoform 4
Serpin A3-1 precursor	Heat shock protein HSP 90-alpha
Hemoglobin subunit alpha	PREDICTED: complement component 4 binding protein, alpha chain-like

(Continued)

Table S2 (*Continued*)

RPMI-bare	RPMI-Si
Alpha-fetoprotein precursor	Apolipoprotein A-II precursor
PREDICTED: similar to complement component 4A	Coagulation factor X
Factor XIIa inhibitor precursor	Elongation factor 1-alpha 2
Neuropilin-2	Pyruvate kinase isozymes M1/M2
Fibrinogen gamma-B chain precursor	Kininogen-2 isoform 1
Nidogen-1	PREDICTED: similar to complement component 4A
Collectin-11 precursor	Heat shock protein HSP 90-beta
Serpin A3-7	Apolipoprotein M
PREDICTED: sushi, von Willebrand factor type A, EGF, and pentraxin domain containing 1, partial	PREDICTED: GLIS family zinc finger 3, partial
Thyroglobulin precursor	Glyceraldehyde-3-phosphate dehydrogenase
Lumican precursor	PREDICTED: putative zinc finger protein ENSP00000330994-like, partial
Complement C5a anaphylatoxin	Vitamin D-binding protein precursor
Collagen alpha-1 (XII) chain	Glyceraldehyde-3-phosphate dehydrogenase, testis-specific
Vitamin D-binding protein precursor	Tubulin alpha-4A chain
Fibromodulin	Hyaluronan-binding protein 2
Pentraxin-related protein PTX3 precursor	Actin, cytoplasmic 1
6-Phosphogluconate dehydrogenase, decarboxylating	Adenosylhomocysteinase
PREDICTED: GLIS family zinc finger 3, partial	Actin, alpha cardiac muscle 1
Neuropilin-1	PREDICTED: hCG1647286-like
PREDICTED: heparan sulfate proteoglycan 2	Transthyretin precursor
Reelin	PREDICTED: calcineurin binding protein 1
Lipopolysaccharide-binding protein precursor	Carboxypeptidase b2 precursor
CTAGE family, member 5	Leucine-rich repeat-containing protein 49
Rab GDP dissociation inhibitor beta	Neural cell adhesion molecule 1 precursor
PREDICTED: VGF nerve growth factor inducible-like	Biglycan precursor
Actin, aortic smooth muscle	Tubulin alpha-1D chain
Eukaroytic elongation factor 2 kinase	PREDICTED: phosphorylase kinase, beta
Thrombospondin-3	C-type lectin domain family 11 member A
von Willebrand factor	Alpha-1-acid glycoprotein precursor
SPARC-like protein 1	Kelch-like ECH-associated protein 1
Alpha-actinin-1	Coagulation factor XIII A chain precursor
Apolipoprotein A-I preproprotein	PREDICTED: cadherin 4, type 1 preproprotein-like
Carbohydrate sulfotransferase 3	PREDICTED: neurofilament, medium polypeptide
Serine/threonine-protein phosphatase 2A 65 kda regulatory subunit A alpha isoform	ATP synthase subunit D, mitochondrial
Actin, cytoplasmic 1	PREDICTED: mcg144546-like
tRNA-dihydrouridine synthase 1-like	Neutrophil cytosol factor 1
Retinoic acid receptor responder (tazarotene induced) 1	Alpha-S1-casein precursor
Interleukin-1 beta precursor	Serpin A3-1 precursor
NACHT, LRR, and PYD domains-containing protein 5	6-Phosphogluconate dehydrogenase, decarboxylating
Hypothetical protein LOC781988	Pigment epithelium-derived factor precursor
Tenascin-X	Serpin A3-7
Heat shock protein HSP 90-alpha	PREDICTED: collagen, type IV, alpha 2, partial
Mannan-binding lectin serine protease 2	Tyrosine-protein kinase BAZ1B
Galectin-3-binding protein precursor	Inner nuclear membrane protein MAN1
Adenosine deaminase-like protein	PREDICTED: NIMA (never in mitosis gene a)-related kinase 11
Ankyrin repeat domain-containing protein 32	Nucleolar GTP-binding protein 2
PREDICTED: hCG1647286-like	Annexin A2
Fatty acid synthase	SPARC-like protein 1
Tenascin C	L-lactate dehydrogenase C isoform 1
Apolipoprotein M	Casein kinase II subunit alpha
Ras-related protein Rap-1b precursor	Glycine N-acyltransferase
Zinc finger protein 366	Fibrinogen alpha chain precursor
PREDICTED: multiple C2 domains, transmembrane 1-like	Peroxisomal biogenesis factor 3

(*Continued*)

Table S2 (*Continued*)

RPMI-bare	RPMI-Si
DnaJ homolog subfamily C member 27	PREDICTED: kinesin family member 13A
Nucleosome assembly protein 1-like 1	Filamin-C
Chromodomain helicase DNA binding protein 6	Heat shock 70 kda protein 1A
PREDICTED: tudor domain-containing protein 12-like	MKL/myocardin-like protein 2
Plasma serine protease inhibitor precursor	Sulfhydryl oxidase 1
Transforming growth factor-beta-induced protein ig-h3	Alpha-1b-glycoprotein precursor
Reversion-inducing cysteine-rich protein with Kazal motifs	PREDICTED: KIAA1747 protein-like
Transcription elongation factor B polypeptide 1	PREDICTED: mkiaa4091 protein-like
PREDICTED: mcg144546-like	Thiamin pyrophosphokinase 1
Aggrecan core protein	Nol1/nop2/sun domain family, member 5
Complement factor B precursor	L-lactate dehydrogenase B chain
PREDICTED: solute carrier family 30 (zinc transporter), member 1-like	Coiled-coil domain-containing protein 50
Pregnancy-associated glycoprotein	PREDICTED: seizure related 6 homolog (mouse)-like
PREDICTED: nebulin	Serotransferrin-like
PREDICTED: suppression of tumorigenicity 18 (breast carcinoma) (zinc finger protein)	NACHT and WD repeat domain-containing protein 1
Leucine-rich repeat-containing protein 49	
PREDICTED: tyrosine-protein phosphatase non-receptor type 21-like	
PREDICTED: olfactory receptor, family 5, subfamily I, member 1-like	
Histamine N-methyltransferase	
PREDICTED: ZAR1-like protein-like	
Regulator of G-protein signaling like 1	
ELKS/Rab6-interacting/CAST family member 1	
Elongation factor Ts, mitochondrial precursor	
Neural cell adhesion molecule 1 precursor	
Homeobox protein Hox-A4	
PREDICTED: dystrotelin-like	
PREDICTED: centromere protein E, 312 kDa	
Importin subunit beta-1	
PREDICTED: apobec-1 complementation factor-like isoform 2	
Choline transporter-like protein 4	
Sperm associated antigen 7	
PREDICTED: similar to uncharacterized protein c10orf90	
Probable ATP-dependent RNA helicase DDX17	
Dnaj homolog subfamily C member 21	
Leucine-rich repeat-containing protein 48	
UTP – glucose-1-phosphate uridylyltransferase	
PREDICTED: FLJ00002 protein-like	
Hephaestin-like protein 1	
Serine/threonine-protein phosphatase PP1-alpha catalytic subunit	
PREDICTED: hypothetical protein	
Acetyl-CoA carboxylase 1	
PREDICTED: zinc finger protein 107-like	
Zinc finger protein 180	
Ribonucleoside-diphosphate reductase M1 chain	
AT-rich interactive domain-containing protein 5A	
Protein farnesyltransferase/geranylgeranyltransferase type-1 subunit alpha	

Abbreviations: Si, silica; ATP, adenosine triphosphate; tRNA, transfer ribonucleic acid; RPMI, Roswell Park Memorial Institute.

Table S3 List of DMEM common proteins involved in both AuNRs and SiO₂-AuNRs

DMEM common
PREDICTED: apolipoprotein B
Alpha-2-macroglobulin
Fibronectin
Complement C3 preproprotein
Inter-alpha-trypsin inhibitor heavy chain H2
Inter-alpha-trypsin inhibitor heavy chain H3 precursor
Serum albumin precursor
Complement C4
Inter-alpha-trypsin inhibitor heavy chain H1 precursor
Fibulin-1
Gelsolin isoform a
Angiotensinogen
Heparin cofactor 2
Alpha-2-HS-glycoprotein precursor
Vitronectin
Prothrombin
Periostin
Antithrombin-III precursor
Alpha-1-antiproteinase precursor
Protein AMBP precursor
Talin-1
Apolipoprotein E precursor
Alpha-2-antiplasmin precursor
Apolipoprotein A-I preproprotein
Hemoglobin fetal subunit beta
C4b-binding protein alpha chain precursor
Kininogen-2 isoform II
Complement component C9 precursor
PREDICTED: apolipoprotein B
PREDICTED: similar to complement component 4A
Hemoglobin subunit beta
Hemoglobin subunit alpha
Hypothetical protein LOC510860
Heat shock protein HSP 90-alpha
Serpin A3-1 precursor
Actin, aortic smooth muscle
Inter-alpha-trypsin inhibitor heavy chain H4 precursor
Apolipoprotein M
PREDICTED: complement component 4 binding protein, alpha chain-like
Heat shock protein HSP 90-beta
Fetuin-B precursor
Vitamin D-binding protein precursor
Plasma serine protease inhibitor precursor
Glyceraldehyde-3-phosphate dehydrogenase
Transmembrane and coiled-coil domain-containing protein 2
Nucleolar GTP-binding protein 2

Abbreviations: DMEM, Dulbecco's Modified Eagle's Medium; AuNRs, gold nanorods; SiO₂-AuNRs, gold nanorods functionalized with silica.

Table S4 List of RPMI common proteins involved in both AuNRs and SiO₂-AuNRs

RPMI common
PREDICTED: apolipoprotein B
Fibronectin
Complement C3 preproprotein
Inter-alpha-trypsin inhibitor heavy chain H2
Alpha-2-macroglobulin
Serum albumin precursor
Inter-alpha-trypsin inhibitor heavy chain H3 precursor
Thrombospondin-1 precursor
Inter-alpha-trypsin inhibitor heavy chain H1 precursor
Gelsolin isoform a
Talin-1
Complement C4
Fibulin-1
PREDICTED: pregnancy-zone protein-like
Angiotensinogen
Thrombospondin-4 precursor
Antithrombin-III precursor
Heparin cofactor 2
Prothrombin
Vitronectin
Inter-alpha-trypsin inhibitor heavy chain H4 precursor
Periostin
Alpha-2-HS-glycoprotein precursor
Alpha-1-antiproteinase precursor
Protein AMBP precursor
Hyaluronan-binding protein 2
Alpha-2-antiplasmin precursor
Coagulation factor V precursor
Tubulin, beta 1
Kininogen-2 isoform II
PREDICTED: apolipoprotein B
PREDICTED: collagen, type VI, alpha 3-like isoform 4
Hemoglobin fetal subunit beta
Kininogen-2 isoform I
Apolipoprotein E precursor
Tubulin alpha-4A chain
Hypothetical protein LOC510860
Heat shock protein HSP 90-beta
C4b-binding protein alpha chain precursor
Hemoglobin subunit beta
Coagulation factor X
PREDICTED: complement component 4 binding protein, alpha chain-like
Fibrinogen beta chain
Complement component C9 precursor
C-type lectin domain family 11 member A
Fetuin-B precursor
Hemoglobin subunit alpha
Alpha-fetoprotein precursor
PREDICTED: similar to complement component 4A
Complement C5a anaphylatoxin
Vitamin D-binding protein precursor
PREDICTED: GLIS family zinc finger 3, partial
Lipopolysaccharide-binding protein precursor
Actin, aortic smooth muscle
Apolipoprotein A-I preproprotein
Actin, cytoplasmic 1
Heat shock protein HSP 90-alpha
PREDICTED: hCG1647286-like
Apolipoprotein M

Abbreviations: AuNRs, gold nanorods; SiO₂-AuNRs, gold nanorods functionalized with silica; RPMI, Roswell Park Memorial Institute.

Table S5 List of DMEM unique proteins involved in either AuNRs or SiO$_2$-AuNRs

DMEM uncommon

DMEM-bare	DMEM-Si
PREDICTED: pregnancy-zone protein-like	Lipopolysaccharide-binding protein precursor
Thrombospondin-1 precursor	Coagulation factor XIII A chain precursor
Thrombospondin-4 precursor	Serotransferrin precursor
Thyroglobulin precursor	Phosphoglycerate kinase 1
Coagulation factor V precursor	Actin, cytoplasmic 1
Hyaluronan-binding protein 2	L-lactate dehydrogenase B chain
Tubulin, beta 1	Apolipoprotein A-II precursor
PREDICTED: heparan sulfate proteoglycan 2	Fermitin family homolog 3
Fibrinogen alpha chain precursor	Phospholipid transfer protein
Factor XIIa inhibitor precursor	Pyruvate kinase isozymes M1/M2
Tubulin alpha-4A chain	Adenosylhomocysteinase
Kininogen-2 isoform 1	Complement component 8, beta polypeptide
Mannan-binding lectin serine protease 1	Kelch-like ECH-associated protein 1
Fibrinogen beta chain	Alpha-enolase
Tenascin-X	Glyceraldehyde-3-phosphate dehydrogenase, testis-specific
Collagen alpha-1 (XII) chain	Probable arginyl-tRNA synthetase, mitochondrial precursor
Tubulin beta-5 chain	L-lactate dehydrogenase C isoform 1
Fibromodulin	Thyroxine-binding globulin precursor
Lumican precursor	Neutrophil cytosol factor 1
Alpha-actinin-1	Apolipoprotein D precursor
Neuropilin-1	
Echinoderm microtubule-associated protein-like 5	
PREDICTED: alpha-2-macroglobulin-like, partial	
Aggrecan core protein	
PREDICTED: GLIS family zinc finger 3, partial	
PREDICTED: calcium channel, voltage-dependent, L type, alpha 1S subunit-like	
Myosin, heavy chain 9, nonmuscle	
Caspase-14	
tRNA-dihydrouridine synthase 1-like	
Myosin-11	
PREDICTED: KRAB-A domain containing 2	
Thrombospondin-3	
Neuropilin-2	
Beta-casein precursor	
PREDICTED: collagen, type VI, alpha 3-like isoform 4	
Sucrase-isomaltase, intestinal	
Complement factor B precursor	
Interleukin-1 beta precursor	
PREDICTED: NIMA (never in mitosis gene a)-related kinase 11	
Coagulation factor X	
SPARC-like protein 1	
PREDICTED: FYVE and coiled-coil domain-containing protein 1-like	
PREDICTED: thiolester containing protein II-like	
Carbohydrate sulfotransferase 3	
PREDICTED: zinc finger protein 347-like	
C-type lectin domain family 11 member A	
Terminal uridylyltransferase 4	
Alpha-S1-casein precursor	
Collectin-11 precursor	
Mannan-binding lectin serine protease 2	
N-acetylated-alpha-linked acidic dipeptidase 2	
Pentraxin-related protein PTX3 precursor	
6-phosphogluconate dehydrogenase, decarboxylating	
Nidogen-1	
Mitochondrial-processing peptidase subunit alpha precursor	
Coiled-coil alpha-helical rod protein 1	

Abbreviations: DMEM, Dulbecco's Modified Eagle's Medium; AuNRs, gold nanorods; SiO$_2$-AuNRs, gold nanorods functionalized with silica; tRNA, transfer ribonucleic acid.

Table S6 List of RPMI unique proteins involved in either AuNRs or SiO$_2$-AuNRs

RPMI uncommon

RPMI-bare	RPMI-Si
Tubulin beta-5 chain	Complement factor B precursor
Pigment epithelium-derived factor precursor	Serotransferrin precursor
Cartilage oligomeric matrix protein	Plasma serine protease inhibitor precursor
Mannan-binding lectin serine protease 1	Fermitin family homolog 3
Fibrinogen alpha chain precursor	Phospholipid transfer protein
Filamin-A	Complement component 8, beta polypeptide
Serpin A3-1 precursor	Properdin
Factor XIIa inhibitor precursor	Apolipoprotein A-II precursor
Neuropilin-2	Elongation factor 1-alpha 2
Fibrinogen gamma-B chain precursor	Pyruvate kinase isozymes M1/M2
Nidogen-1	Glyceraldehyde-3-phosphate dehydrogenase
Collectin-11 precursor	PREDICTED: Putative zinc finger protein
	ENSP00000330994-like, partial
Serpin A3-7	Glyceraldehyde-3-phosphate dehydrogenase, testis-specific
PREDICTED: sushi, von Willebrand factor type A, EGF,	Adenosylhomocysteinase
and pentraxin domain containing 1, partial	
Thyroglobulin precursor	Actin, alpha cardiac muscle 1
Lumican precursor	Transthyretin precursor
Collagen alpha-1 (XII) chain	PREDICTED: calcineurin binding protein 1
Fibromodulin	Carboxypeptidase B2 precursor
Pentraxin-related protein PTX3 precursor	Leucine-rich repeat-containing protein 49
6-phosphogluconate dehydrogenase, decarboxylating	Neural cell adhesion molecule 1 precursor
Neuropilin-1	Biglycan precursor
PREDICTED: heparan sulfate proteoglycan 2	Tubulin alpha-1D chain
Reelin	PREDICTED: phosphorylase kinase, beta
CTAGE family, member 5	Alpha-1-acid glycoprotein precursor
Rab GDP dissociation inhibitor beta	Kelch-like ECH-associated protein 1
PREDICTED: VGF nerve growth factor inducible-like	
Eukaroytic elongation factor 2 kinase	
Thrombospondin-3	
von Willebrand factor	
SPARC-like protein 1	
Alpha-actinin-1	
Carbohydrate sulfotransferase 3	
Serine/threonine-protein phosphatase 2A 65 kDa regulatory	
subunit A alpha isoform	
tRNA-dihydrouridine synthase 1-like	
Retinoic acid receptor responder (tazarotene induced) 1	
Interleukin-1 beta precursor	
NACHT, LRR, and PYD domains-containing protein 5	
Hypothetical protein LOC781988	
Tenascin-X	
Mannan-binding lectin serine protease 2	
Galectin-3-binding protein precursor	
Adenosine deaminase-like protein	
Ankyrin repeat domain-containing protein 32	
Fatty acid synthase	
Tenascin C	
Ras-related protein Rap-1b precursor	
Zinc finger protein 366	

Abbreviations: AuNRs, gold nanorods; SiO$_2$-AuNRs, gold nanorods functionalized with silica; Si, silica; tRNA, transfer ribonucleic acid; RPMI, Roswell Park Memorial Institute.

Table S7 List of AuNRs attached common proteins involved in both DMEM and RPMI

BARE common

PREDICTED: apolipoprotein B

Alpha-2-macroglobulin

Fibronectin

Complement C3 preproprotein

Inter-alpha-trypsin inhibitor heavy chain H2

Inter-alpha-trypsin inhibitor heavy chain H3 precursor

Serum albumin precursor

Complement C4

Inter-alpha-trypsin inhibitor heavy chain H1 precursor

Fibulin-1

PREDICTED: pregnancy-zone protein-like

Gelsolin isoform a

Thrombospondin-1 precursor

Angiotensinogen

Heparin cofactor 2

Alpha-2-HS-glycoprotein precursor

Vitronectin

Prothrombin

Periostin

Thrombospondin-4 precursor

Antithrombin-III precursor

Alpha-1-antiproteinase precursor

Protein AMBP precursor

Talin-1

Thyroglobulin precursor

Apolipoprotein E precursor

Alpha-2-antiplasmin precursor

Apolipoprotein A-I preproprotein

Hemoglobin fetal subunit beta

Coagulation factor V precursor

Hyaluronan-binding protein 2

C4b-binding protein alpha chain precursor

Kininogen-2 isoform II

Complement component C9 precursor

PREDICTED: apolipoprotein B

Tubulin, beta 1

PREDICTED: similar to complement component 4A

PREDICTED: heparan sulfate proteoglycan 2

Hemoglobin subunit beta

Fibrinogen alpha chain precursor

Hemoglobin subunit alpha

Hypothetical protein LOC510860

(Continued)

Table S7 (*Continued*)

BARE common

Heat shock protein HSP 90-alpha

Serpin A3-1 precursor

Factor XIIa inhibitor precursor

Actin, aortic smooth muscle

Tubulin alpha-4A chain

Kininogen-2 isoform I

Inter-alpha-trypsin inhibitor heavy chain H4 precursor

Mannan-binding lectin serine protease 1

Apolipoprotein M

Fibrinogen beta chain

Tenascin-X

PREDICTED: complement component 4 binding protein, alpha chain-like

Collagen alpha-1 (XII) chain

Heat shock protein HSP 90-beta

Tubulin beta-5 chain

Fibromodulin

Fetuin-B precursor

Lumican precursor

Alpha-actinin-1

Vitamin D-binding protein precursor

Neuropilin-1

PREDICTED: GLIS family zinc finger 3, partial

tRNA-dihydrouridine synthase 1-like

Thrombospondin-3

Neuropilin-2

PREDICTED: collagen, type VI, alpha 3-like isoform 4

Interleukin-1 beta precursor

Coagulation factor X

SPARC-like protein 1

Carbohydrate sulfotransferase 3

C-type lectin domain family 11 member A

Collectin-11 precursor

Mannan-binding lectin serine protease 2

Pentraxin-related protein PTX3 precursor

6-phosphogluconate dehydrogenase, decarboxylating

Nidogen-1

Abbreviations: AuNRs, gold nanorods; DMEM, Dulbecco's Modified Eagle's Medium; tRNA, transfer ribonucleic acid; RPMI, Roswell Park Memorial Institute.

1542

International Journal of Nanomedicine 2015:10

Table S8 List of SiO$_2$-AuNRs attached common proteins involved in both DMEM and RPMI

Si common

PREDICTED: apolipoprotein B
Complement C3 preproprotein
Serum albumin precursor
Alpha-2-macroglobulin
Antithrombin-III precursor
Apolipoprotein E precursor
Inter-alpha-trypsin inhibitor heavy chain H2
Apolipoprotein A-I preproprotein
Fibulin-1
Alpha-1-antiproteinase precursor
Alpha-2-HS-glycoprotein precursor
Complement C4
Periostin
Inter-alpha-trypsin inhibitor heavy chain H3 precursor
Hemoglobin subunit alpha
Vitronectin
Heparin cofactor 2
Prothrombin
Inter-alpha-trypsin inhibitor heavy chain H4 precursor
Hemoglobin fetal subunit beta
Angiotensinogen
PREDICTED: complement component 4 binding protein, alpha chain-like
Gelsolin isoform a
Protein AMBP precursor
Fetuin-B precursor
Lipopolysaccharide-binding protein precursor
Plasma serine protease inhibitor precursor
Complement component C9 precursor
Actin, aortic smooth muscle

(*Continued*)

Table S8 (*Continued*)

Si common

Talin-1
PREDICTED: apolipoprotein B
Serotransferrin precursor
Hemoglobin subunit beta
Alpha-2-antiplasmin precursor
Inter-alpha-trypsin inhibitor heavy chain H1 precursor
Actin, cytoplasmic 1
Apolipoprotein A-II precursor
Fibronectin
Hypothetical protein LOC510860
Heat shock protein HSP 90-beta
Fermitin family homolog 3
Phospholipid transfer protein
Pyruvate kinase isozymes M1/M2
Adenosylhomocysteinase
Complement component 8, beta polypeptide
Kininogen-2 isoform II
Kelch-like ECH-associated protein 1
Apolipoprotein M
Glyceraldehyde-3-phosphate dehydrogenase
Glyceraldehyde-3-phosphate dehydrogenase, testis-specific
Vitamin D-binding protein precursor
Heat shock protein HSP 90-alpha
C4b-binding protein alpha chain precursor

Abbreviations: SiO$_2$-AuNRs, gold nanorods functionalized with silica; Si, silica; DMEM, Dulbecco's Modified Eagle's Medium; RPMI, Roswell Park Memorial Institute.

Table S9 List of AuNRs attached unique proteins involved in either DMEM or RPMI

Bare uncommon

DMEM-bare	RPMI-bare
Echinoderm microtubule-associated protein-like 5	Pigment epithelium-derived factor precursor
PREDICTED: alpha-2-macroglobulin-like, partial	Cartilage oligomeric matrix protein
Aggrecan core protein	Filamin-A
Plasma serine protease inhibitor precursor	Alpha-fetoprotein precursor
PREDICTED: calcium channel, voltage-dependent, L type, alpha 1S subunit-like	Fibrinogen gamma-B chain precursor
Myosin, heavy chain 9, nonmuscle	Serpin A3-7
Glyceraldehyde-3-phosphate dehydrogenase	PREDICTED: sushi, von Willebrand factor type A, EGF, and pentraxin domain containing 1, partial
Caspase-14	Complement C5a anaphylatoxin
Myosin-11	Reelin
PREDICTED: KRAB-A domain containing 2	Lipopolysaccharide-binding protein precursor
Beta-casein precursor	CTAGE family, member 5
Sucrase-isomaltase, intestinal	Rab GDP dissociation inhibitor beta
Transmembrane and coiled-coil domain-containing protein 2	PREDICTED: VGF nerve growth factor inducible-like
Complement factor B precursor	Eukaroytic elongation factor 2 kinase
PREDICTED: NIMA (never in mitosis gene a)-related kinase 11	von Willebrand factor
PREDICTED: FYVE and coiled-coil domain-containing protein 1-like	Serine/threonine-protein phosphatase 2A 65 kDa regulatory subunit A alpha isoform
PREDICTED: thiolester containing protein II-like	Actin, cytoplasmic 1
PREDICTED: zinc finger protein 347-like	Retinoic acid receptor responder (tazarotene induced) 1
Terminal uridylyltransferase 4	NACHT, LRR, and PYD domains-containing protein 5
Nucleolar GTP-binding protein 2	Hypothetical protein LOC781988
Alpha-S1-casein precursor	Galectin-3-binding protein precursor
N-acetylated-alpha-linked acidic dipeptidase 2	Adenosine deaminase-like protein
Mitochondrial-processing peptidase subunit alpha precursor	Ankyrin repeat domain-containing protein 32
Coiled-coil alpha-helical rod protein 1	PREDICTED: hCG1647286-like
	Fatty acid synthase
	Tenascin C
	Ras-related protein Rap-1b precursor
	Zinc finger protein 366

Abbreviations: AuNRs, gold nanorods; DMEM, Dulbecco's Modified Eagle's Medium; RPMI, Roswell Park Memorial Institute.

Table S10 List of SiO$_2$-AuNRs attached unique proteins involved in either DMEM or RPMI

Si uncommon

DMEM-Si	RPMI-Si
Coagulation factor XIII A chain precursor	PREDICTED: pregnancy-zone protein-like
Phosphoglycerate kinase 1	Complement factor B precursor
L-lactate dehydrogenase B chain	Tubulin, beta 1
Alpha-enolase	Complement C5a anaphylatoxin
Transmembrane and coiled-coil domain-containing protein 2	Thrombospondin-1 precursor
Probable arginyl-tRNA synthetase, mitochondrial precursor	Fibrinogen beta chain
Serpin A3-1 precursor	Alpha-fetoprotein precursor
L-lactate dehydrogenase C isoform 1	Thrombospondin-4 precursor
Nucleolar GTP-binding protein 2	Properdin
Thyroxine-binding globulin precursor	Coagulation factor V precursor
Neutrophil cytosol factor 1	PREDICTED: collagen, type VI, alpha 3-like isoform 4
Apolipoprotein D precursor	Coagulation factor X
	Elongation factor 1-alpha 2
	Kininogen-2 isoform 1
	PREDICTED: GLIS family zinc finger 3, partial
	PREDICTED: Putative zinc finger protein ENSP00000330994-like, partial
	Tubulin alpha-4A chain
	Hyaluronan-binding protein 2
	Actin, alpha cardiac muscle 1
	PREDICTED: hCG1647286-like
	Transthyretin precursor
	PREDICTED: calcineurin binding protein 1
	Carboxypeptidase B2 precursor
	Leucine-rich repeat-containing protein 49
	Neural cell adhesion molecule 1 precursor
	Biglycan precursor
	Tubulin alpha-1D chain
	PREDICTED: phosphorylase kinase, beta
	C-type lectin domain family 11 member A
	Alpha-1-acid glycoprotein precursor

Abbreviations: SiO$_2$-AuNRs, gold nanorods functionalized with silica; DMEM, Dulbecco's Modified Eagle's Medium; Si, silica; tRNA, transfer ribonucleic acid; RPMI, Roswell Park Memorial Institute.